ISSN: 2664-9640

Optimization of Point-Loaded Bragg Gratings based on Equivalent Apodization

Boyi Liang*

School of Electronic and Information Engineering, Beijing Jiaotong University, Beijing 100044, China

*Corresponding author's e-mail: KiraCaram@163.com

Abstract

Silicon nitride integrated waveguides have attracted considerable attention in integrated photonic devices due to their low propagation loss, broad optical transparency window, and excellent compatibility with mature fabrication processes. Integrated waveguide gratings, as key components for on-chip wavelength selection and optical feedback control, play an important role in determining the spectral characteristics of filters and feedback structures. In this work, an equivalent apodization model for point-loaded Bragg gratings is developed based on coupled-mode theory and the transfer matrix method. By introducing a spatially varying coupling coefficient, the discrete modulation of the point-loaded grating can be described using a unified analytical model. MATLAB simulations are then performed for both uniform and apodized gratings to examine how different apodization profiles affect the reflection spectrum, with particular attention to sidelobe suppression and spectral characteristics. The simulation results show that apodization can effectively suppress sidelobes and produce a smoother reflection response, while the central Bragg wavelength remains essentially unchanged. Among the profiles considered in this study, the Gaussian function offers a relatively good balance between main-peak reflectivity and sidelobe suppression. This equivalent modeling method therefore provides a practical theoretical framework for analyzing the spectral response of point-loaded integrated Bragg gratings and for further optimization of their performance.

Keywords

Integrated Waveguide Grating; Point-Loaded Bragg Grating; Apodization; Transfer Matrix Method; Equivalent Apodization Model.

1. Introduction

With the continuous development of integrated photonics, optical waveguide devices based on silicon and silicon nitride platforms have been widely applied in high-speed optical communication, on-chip optical interconnects, optical sensing, and integrated light sources[1]. Owing to their compact footprint, low loss, and compatibility with complementary metal–oxide–semiconductor (CMOS) processes, integrated optical waveguide devices have gradually become an important research direction in optoelectronic devices. Among them, Bragg gratings, as typical one-dimensional periodic structures, can achieve wavelength-selective reflection of specific wavelengths through periodic refractive-index modulation[2]. Therefore, they are widely used in key functional modules such as filter design, laser feedback cavities, and spectral control.

Conventional uniform Bragg gratings typically employ a constant refractive-index modulation depth and a fixed grating period throughout the device. Consequently, the coupling strength drops abruptly at the two ends of the grating. From the spectral perspective, this sharp

ISSN: 2664-9640

truncation can be regarded as a rectangular window imposed on the spatial distribution of the coupling coefficient, thereby introducing additional high-spatial-frequency components. These components give rise to sidelobes around the main reflection peak. The resulting spectral broadening reduces the concentration of reflected power near the target wavelength and can also affect the wavelength-selective feedback of the grating. This issue is particularly relevant to external-cavity lasers, where unwanted feedback at nearby wavelengths may promote mode competition and adversely affect the stability of laser operation.

Apodization provides a way to alleviate these spectral effects by modifying the coupling strength along the grating. Instead of keeping the coupling coefficient constant throughout the whole structure, the grating strength is allowed to change gradually along the propagation direction. In particular, a reduction in coupling strength near the two ends produces a smoother transition between the grating and the surrounding unmodulated waveguide. This reduces the spectral oscillations associated with the abrupt boundaries and leads to a more regular reflection response. In analytical models, such a variation is commonly represented by introducing a spatial weighting function into the coupling coefficient. When incorporated into coupled-mode theory or the transfer matrix method, the resulting model can be used to quantitatively evaluate the reflection and transmission characteristics of apodized gratings.

2. Literature Review

Fiber Bragg gratings have evolved from early reflection-type filtering structures into engineerable periodic refractive-index modulation structures. In recent years, research on Bragg gratings and their optimization has mainly focused on several aspects, including coupled-mode-theory-based modeling, apodization optimization methods, and the structural implementation of integrated optical waveguide gratings. In terms of theoretical research, Erdogan systematically established the coupled-mode theory model for fiber Bragg gratings, laying an important foundation for analytical calculation and physical mechanism analysis of grating reflection spectra[3]. On this basis, researchers have further introduced numerical analysis methods such as the transfer matrix method to achieve more refined modeling and calculation of the reflection and transmission characteristics of gratings.

In terms of structural optimization, apodization has been widely applied to improve grating performance[4]. Different apodization profiles, including Gaussian, cosine, and exponential functions, can be used to tailor the spatial variation of the grating coupling coefficient. By replacing the abrupt coupling distribution with a gradual one, these profiles can reduce sidelobes in the reflection spectrum and improve the wavelength selectivity of the grating. Their use has become well established in fiber Bragg grating design, where apodization is commonly employed to obtain a cleaner spectral response and better suppression of unwanted spectral components.

For integrated devices, Bragg gratings fabricated on silicon and silicon nitride waveguide platforms have been investigated in a variety of configurations. The specific grating structure depends on factors such as the fabrication process and the intended device function, and may take the form of point-loaded gratings, sidewall-etched gratings, or loaded-waveguide gratings. These structures can be integrated within planar photonic circuits, while their spectral characteristics can be adjusted through parameters including the grating period, perturbation size, duty cycle, and interaction length. As a result, integrated waveguide gratings have been applied to functions such as on-chip filtering, wavelength selection, and optical feedback in external-cavity systems.

However, the apodization design of point-loaded Bragg gratings still requires further analysis. Existing studies on apodized gratings mainly focus on continuous or quasi-continuous refractive-index modulation. For point-loaded gratings, the refractive-index perturbation is

ISSN: 2664-9640

introduced by discrete loading units, and the relationship between the discrete structure and the equivalent coupling coefficient is less direct. In addition, many apodization designs are based on empirical adjustment of geometric parameters. A unified model that can describe different apodization profiles under the same theoretical framework is therefore useful for comparing their spectral effects. In particular, the influence of different apodization functions on sidelobe suppression, reflection bandwidth, and peak reflectivity has not been sufficiently compared for point-loaded grating structures[5].

Based on this consideration, this work models the point-loaded Bragg grating through an equivalent apodization approach. Under the coupled-mode-theory framework, the effect of discrete structural perturbations is represented by a spatially varying coupling coefficient. The transfer matrix method is then used to calculate the reflection and transmission spectra of both uniform and apodized gratings. On this basis, several typical apodization functions are compared under the same grating parameters, with emphasis on their effects on sidelobe suppression and bandwidth characteristics[6].

The contribution of this work lies in the following aspects. First, an equivalent apodization model is introduced for point-loaded Bragg gratings, so that discrete structural modulation can be analyzed through a continuous coupling coefficient distribution. Second, a transfer-matrix-based calculation framework is established for comparing uniform and apodized gratings. Third, the spectral performance of Gaussian, linear, cosine, and exponential apodization functions is evaluated in terms of peak reflectivity, bandwidth, and sidelobe suppression. The results provide a theoretical reference for the design and optimization of point-loaded integrated waveguide gratings[7].

3. Theoretical Model

3.1. Model of the Point-Loaded Bragg Grating

A point-loaded Bragg grating is an integrated optical waveguide structure that realizes Bragg reflection through discrete refractive-index perturbations. Its basic principle is to periodically introduce local refractive-index variations along the propagation direction, thereby satisfying the phase-matching condition at a specific wavelength and enabling wavelength-selective reflection and transmission control.

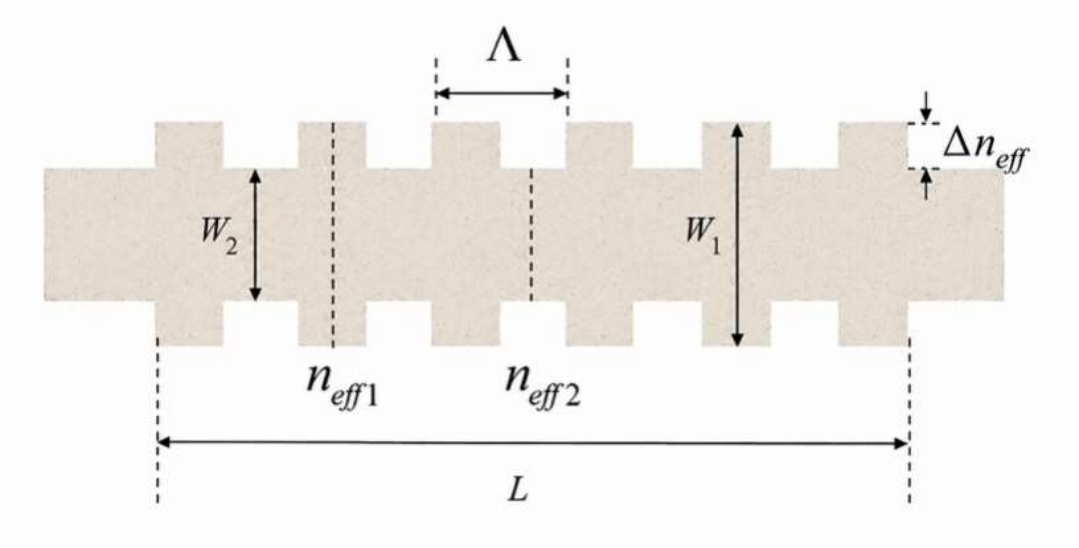


Figure 1. Schematic diagram of a uniform point-loaded grating waveguide

ISSN: 2664-9640

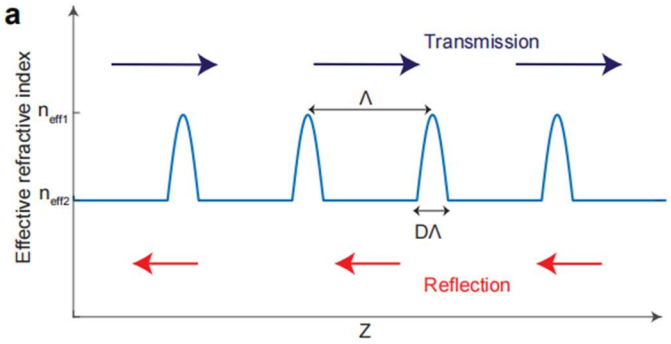


Figure 2. Schematic diagram of local refractive-index modulation in a point-loaded grating

Within the framework of coupled-mode theory, the feedback strength of the grating can be equivalently expressed as a coupling coefficient function varying along the propagation direction, which can be written as:

$$\kappa(z) = \kappa_0 f(z) \tag{1}$$

where κ_0 denotes the average coupling coefficient of the uniform grating, and f(z) is the spatial modulation function used to describe the influence of the point-loaded structure on the optical coupling strength at different positions. When f(z)=1, the structure corresponds to a uniform Bragg grating; when f(z) varies along the propagation direction, it corresponds to an apodized or non-uniform grating structure.

3.2. Bragg Condition

The central reflection wavelength of a Bragg grating is determined by the phase-matching condition, and its basic expression is given by:

$$\lambda_B = 2n_{eff}\Lambda \tag{2}$$

where λ_B is the Bragg wavelength, n_{eff} is the effective refractive index of the waveguide, and Λ is the grating period.

This condition indicates that, when the incident light satisfies a specific wavelength condition, phase matching occurs between the forward-propagating mode and the backward-scattered mode, resulting in strong reflection.

In practical integrated optical waveguide structures, the effective refractive index is affected by the waveguide geometry and material distribution. Therefore, this relationship determines the central operating wavelength of the grating[8].

3.3. Transfer Matrix Method

To analyze the reflection and transmission characteristics of finite-length grating structures, the transfer matrix method is adopted in this work for numerical modeling.

The basic idea of this method is to divide the continuous grating along the propagation direction into multiple small uniform sections. Each section can be described by a 2×2 matrix that represents the propagation relationship of the electric field. For the i-th section, the transfer relation can be expressed as:

ISSN: 2664-9640

$$\begin{bmatrix} E_{i+1}^{+} \\ E_{i+1}^{-} \end{bmatrix} = \begin{bmatrix} M_{11} & M_{12} \\ M_{21} & M_{22} \end{bmatrix} \begin{bmatrix} E_{i}^{+} \\ E_{i}^{-} \end{bmatrix} \tag{3}$$

where E_i^+ and E_i^- denote the forward- and backward-propagating field components, respectively, and M_i is the transfer matrix of the corresponding section.

By multiplying the matrices of all sections in sequence, the total transfer matrix of the entire grating structure can be obtained as:

$$M_{\text{total}} = \prod_{i=1}^{N} M_i \tag{4}$$

The reflection and transmission coefficients can then be calculated, from which the reflection and transmission spectra of the grating are obtained.

This method has good numerical stability and clear physical meaning, making it particularly suitable for the numerical analysis of non-uniform gratings, such as apodized gratings and chirped gratings[9].

3.4. Apodization Function Model

The core idea of apodization is to modulate the spatial distribution of the grating coupling coefficient, so that the abrupt structures at both ends of the grating gradually transition into a smoothly varying distribution. This reduces the high-frequency components in the spectral domain and suppresses the sidelobes in the reflection spectrum.

In this work, different types of apodization functions f(z) are introduced to describe the spatial modulation characteristics of the coupling coefficient. The four main forms considered are as follows:

(1)Gaussian apodization function

$$f(z) = \exp\left[-\left(\frac{z - L/2}{\sigma} \right)^2 \right] \tag{5}$$

This function provides stronger coupling in the central region and gradually decreases toward both ends, exhibiting good sidelobe suppression capability.

(2)Linear apodization function

$$f(z) = az + b \tag{6}$$

This function makes the coupling coefficient vary linearly along the propagation direction. It is easy to implement structurally, but its spectral smoothness is relatively weak.

(3)Cosine apodization function

$$f(z) = \cos^2\left(\frac{\pi z}{L} \right) \tag{7}$$

ISSN: 2664-9640

The cosine-type apodization varies smoothly in the central region and gradually transitions toward both ends, providing a trade-off between bandwidth and sidelobe suppression.

(4)Exponential apodization function

$$f(z) = \exp(-\alpha z) \tag{8}$$

The exponential apodization decays rapidly toward both ends, providing strong suppression of boundary-induced reflection, but it may also reduce the energy of the main reflection peak.

3.5. Summary of This Section

By introducing the spatial modulation function of the coupling coefficient, the physical behaviors of uniform and non-uniform gratings can be described within a unified theoretical framework. Combined with the transfer matrix method, the reflection spectral characteristics of gratings under different apodization functions can be quantitatively analyzed, providing a theoretical basis for subsequent numerical simulation and structural optimization.

4. Simulation Method

4.1. Waveguide Structure and Simulation Parameter Settings

To investigate the spectral response of point-loaded Bragg gratings under different apodization conditions, a numerical model based on coupled-mode theory and the transfer matrix method is established in MATLAB. Since the coupling strength of point-loaded gratings originates from the perturbation of the guided mode induced by periodic structural loading, the waveguide geometry and the corresponding effective refractive index need to be determined before constructing the grating model.

Silicon nitride is selected as the waveguide core material, while silicon dioxide is used as the upper and lower cladding material. Silicon nitride has attracted considerable interest in integrated photonics due to its low propagation loss, broad optical transparency window, and compatibility with CMOS fabrication processes[10]. These characteristics make silicon nitride suitable for low-loss passive feedback structures as well as integrated devices for wavelength selection.

A strip silicon nitride waveguide is used in the present design. The cross-sectional dimensions are chosen with consideration of commonly used low-loss silicon nitride platforms and the integration requirements of the point-loaded grating. The silicon nitride layer has a thickness of 200 nm, while the waveguide width is set to 2500 nm. With these dimensions, the guided mode remains sufficiently confined while an adequate interaction region is retained for the periodic loading structures.

The dimensions of the waveguide have a direct effect on both mode confinement and effective refractive index. When the cross section is reduced, a larger fraction of the optical field extends into the cladding, which weakens the interaction between the guided mode and the loading structures. On the other hand, increasing the waveguide dimensions excessively may allow higher-order modes to propagate and consequently complicate the feedback response of the grating. The selected dimensions are therefore used as a compromise between fundamental-mode confinement, structural feasibility, and the modulation efficiency of the grating.

Using the waveguide geometry described above, an eigenmode analysis is carried out in COMSOL Multiphysics. The calculated fundamental-mode field distribution and effective refractive index are then used in the subsequent grating analysis. For a guided mode propagating along the z direction, the effective refractive index is defined as:

ISSN: 2664-9640

$$n_{\text{eff}} = \frac{\beta}{k_0} \tag{9}$$

where β is the propagation constant of the mode and k_0 is the free-space wave number.

At the operating wavelength of 1550 nm, the TE fundamental mode calculated by COMSOL gives an effective refractive index of:

$$n_{\text{eff}} = 1.5561$$

This value is subsequently used for the calculation of the Bragg condition and the phase detuning term in the transfer matrix model.

For point-loaded Bragg gratings, the refractive-index modulation does not originate from a direct periodic variation of the material refractive index. Instead, it results from the modification of the local optical mode distribution caused by periodic loading structures. Therefore, an equivalent refractive-index modulation term Δn_{eff} is introduced to describe the coupling strength variation induced by the point-loaded structures:

$$\Delta n_{\text{eff}} = n_{\text{eff,loaded}} - n_{\text{eff,bare}} \tag{10}$$

where $n_{\text{eff,loaded}}$ represents the effective refractive index of the waveguide with point-loaded structures, and $n_{\text{eff,bare}}$ corresponds to the unloaded waveguide.

Based on the previous mode simulation results, the equivalent refractive-index modulation depth is set as:

$$\Delta n_{\text{eff}} = 0.0007$$

This parameter is used to calculate the grating coupling coefficient:

$$\kappa = \frac{\pi \Delta n_{\text{eff}}}{\lambda_B} \tag{11}$$

where λ_B denotes the Bragg wavelength.

The grating is designed around a central wavelength of 1550 nm. This wavelength is used as the reference point for evaluating the spectral response of the structure. The total grating length is set to 1 mm, and the resulting model is used to compare the effects of different apodization profiles on sidelobe suppression, peak reflectivity, and spectral bandwidth. A 1 mm grating is adopted to keep the numerical model computationally manageable while retaining the main spectral features needed for a meaningful comparison among the different apodization cases.

The main simulation parameters are set as follows:

Total grating length: 1mm

Effective refractive index: n_{eff} =1.5561

Refractive-index modulation depth: $\Delta n = 7 \times 10^{-4}$

Operating wavelength range: 1549nm – 1551nm

ISSN: 2664-9640

Central wavelength: 1550nm

Number of spatial segments: 200

The number of spatial segments determines the accuracy of the transfer matrix calculation. A larger number of segments provides a closer approximation to a continuously varying coupling coefficient distribution, but also increases the computational cost. Therefore, 200 segments are selected in this work to achieve a balance between numerical accuracy and calculation efficiency.

4.2. Simulation Procedure

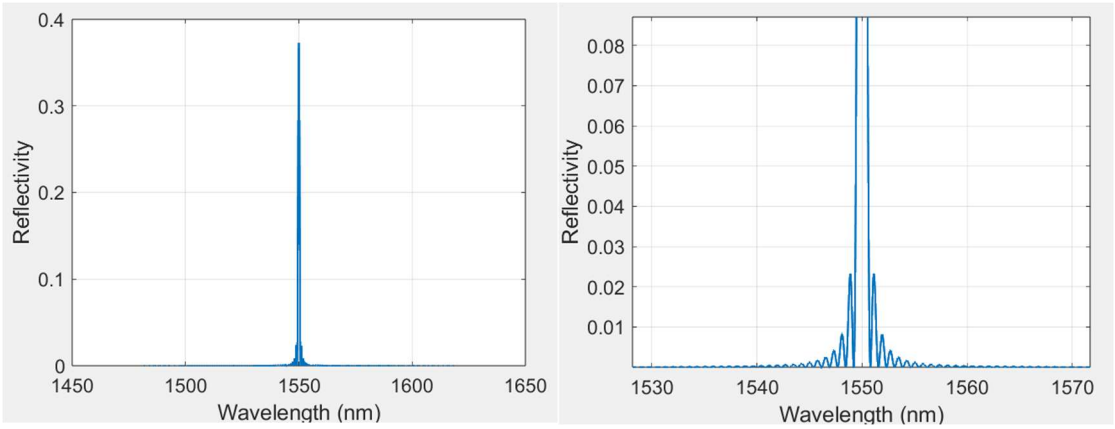
In this work, an equivalent transfer matrix method based on coupled-mode theory is used for the numerical analysis of the grating structure. The main procedure is as follows.

First, a uniform point-loaded Bragg grating model is constructed, in which the refractive-index modulation is treated as a periodic discrete perturbation. Then, a spatially varying coupling coefficient function $\kappa(z)$ is introduced to describe the non-uniform distribution of grating strength under the apodization effect. Subsequently, the grating is divided into multiple small uniform sections, and each section is calculated step by step using a 2×2 transfer matrix. Finally, the reflection and transmission responses of the whole system are obtained through matrix multiplication.

After completing the propagation calculation, the reflection and transmission spectra are extracted and normalized to facilitate quantitative comparison among different structures.

5. Results and Analysis

5.1. Reflection Spectrum of the Uniform Grating



(a) (b)

Figure 3. Reflection spectrum of the uniform grating

The reflection response of the uniform Bragg grating is calculated first as the reference case. Since the refractive-index modulation depth is kept constant along the grating, the coupling coefficient changes abruptly at the two boundaries. As shown in Fig. 3(a), a clear reflection peak is observed near 1550 nm over the selected wavelength range. This peak is consistent with the expected Bragg phase-matching condition and confirms the wavelength-selective response of the grating at the design wavelength.

A magnified view of the spectrum near the central wavelength is given in Fig. 3(b). Several smaller peaks can be observed on either side of the main reflection peak. The oscillatory features are associated with the sharp termination of the grating modulation at its two ends. In other words, the abrupt change in coupling strength at the boundaries contributes directly to the sidelobe structure.

ISSN: 2664-9640

The origin of these sidelobes can also be considered in the spatial-frequency domain. For the uniform grating, the coupling coefficient is approximately constant over the grating length and drops rapidly outside this region, giving a spatial profile similar to a rectangular window. The discontinuities at the two ends introduce additional high-frequency components into the spectral response. These components appear as sidelobes around the principal reflection peak, as illustrated in Fig. 3(b), and distribute part of the reflected power away from the target wavelength.

The presence of these spectral oscillations can affect the wavelength selectivity of the grating and may also produce unwanted feedback at wavelengths adjacent to the main reflection band. This provides the motivation for modifying the spatial distribution of the coupling coefficient. In the following analysis, apodization is introduced to reduce the boundary discontinuities and examine its effect on the resulting spectral response.

5.2. Reflection Spectra of Apodized Gratings

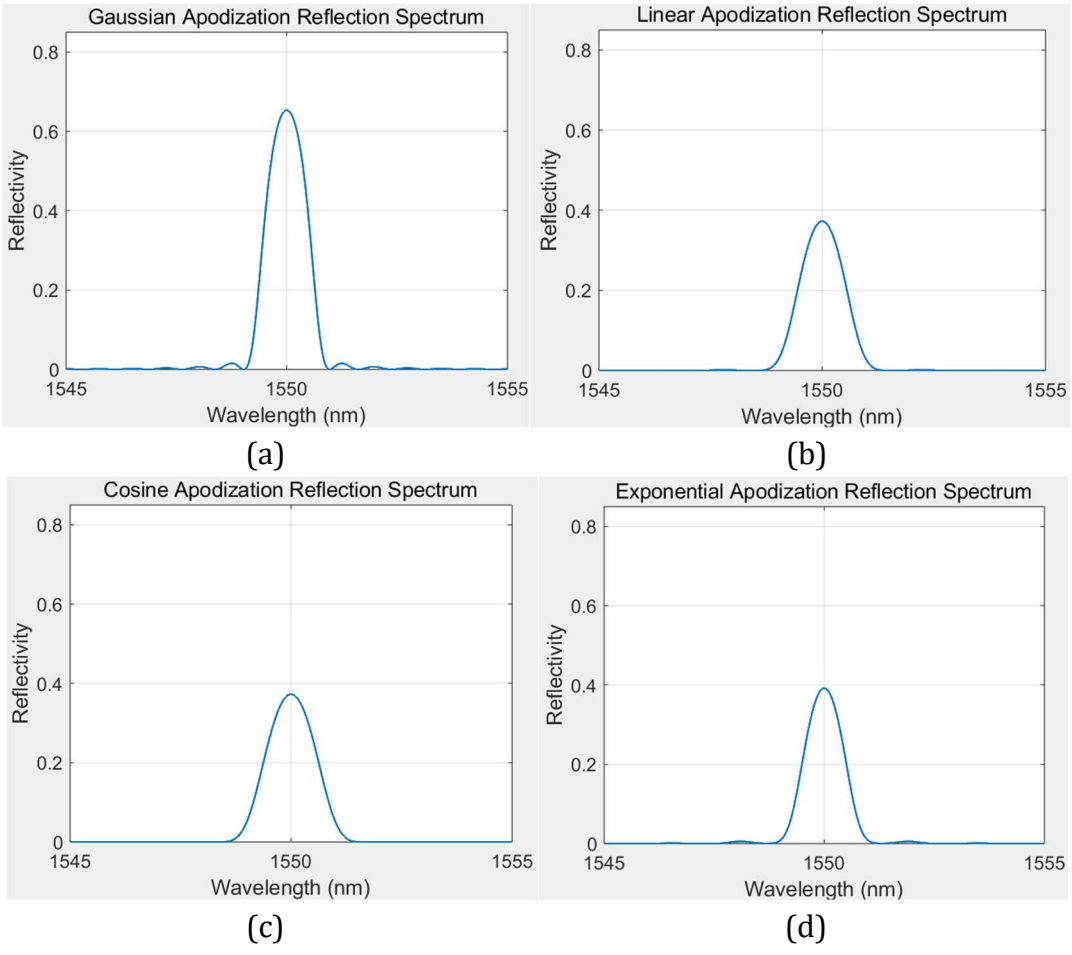


Figure 4. Reflection spectra of four apodized gratings

Starting from the uniform grating model, four apodization profiles are applied to the spatial distribution of the coupling coefficient. In contrast to the uniform case, where the coupling strength is constant within the grating, the apodized structures gradually weaken the coupling toward the two ends. The resulting spatial profile is therefore less abrupt, which helps to reduce oscillations in the reflection spectrum.

The corresponding reflection spectra are plotted in Fig. 4. The result for the Gaussian-apodized grating is given in Fig. 4(a). Its coupling coefficient changes smoothly along the propagation direction, while the central portion of the grating retains a relatively strong coupling strength.

ISSN: 2664-9640

Consequently, the main reflection peak remains comparatively high and the sidelobes are effectively reduced.

The linear-apodized case is shown in Fig. 4(b). Here, the coupling strength changes linearly along the grating, giving a relatively simple spatial distribution. Compared with the Gaussian profile, however, a larger portion of the grating experiences reduced coupling. The main reflection peak is therefore lower under the same simulation conditions.

Figure 4(c) presents the spectrum obtained with cosine apodization. The cosine profile produces a smoother variation near the two boundaries than the linear profile. At the parameter values used in this study, however, the coupling strength is reduced sufficiently over the grating that the reflected power is also lowered. This is reflected in the weaker main peak.

The exponential-apodized result is shown in Fig. 4(d). The coupling coefficient decreases more rapidly near the grating boundaries, which leads to stronger suppression of the sidelobe oscillations. At the same time, this rapid reduction shortens the effective region over which strong coupling takes place, and the main reflection peak is consequently reduced.

Taken together, the four spectra show that apodization changes the spectral response in different ways while leaving the reflection center close to 1550 nm. The main differences appear in peak reflectivity, bandwidth, and sidelobe behavior. Under the present model, these changes are mainly associated with the spatial redistribution of the coupling coefficient, whereas the central Bragg wavelength remains governed primarily by the effective refractive index and grating period.

Therefore, the selection of an appropriate apodization function requires a trade-off between reflection efficiency, spectral bandwidth, and sidelobe suppression. The Gaussian apodization provides a relatively balanced spectral response under the investigated conditions and is therefore considered a suitable candidate for point-loaded Bragg grating optimization.

5.3. Comparison of Reflection Spectrum Performance Parameters for Different Apodization Functions

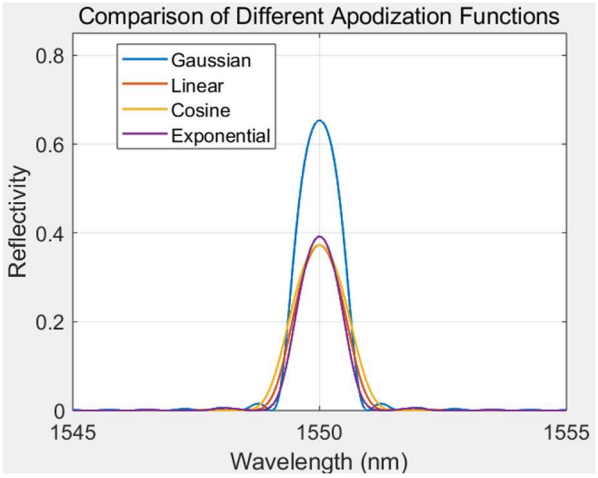


Figure 5. Comparison of reflection spectrum performance parameters for different apodization functions

To further compare the influence of different apodization functions on the reflection spectral performance, Gaussian, linear, cosine, and exponential apodization functions are used in the simulations. The peak reflectivity, 3-dB bandwidth, maximum sidelobe, and sidelobe suppression ratio corresponding to each apodization function are listed in the following table.

ISSN: 2664-9640

Table 1. Comparison of reflection spectrum performance parameters for different apodization functions

Apodization	Rmax	λ_B/nm	FWHM /nm	MaxSidelobe	SLSR /dB
Gaussian	0.65327	1550	1.0819	0.015193	16.334
Linear	0.37246	1550	1.1613	0.011692	15.032
Cosine	0.37246	1550	1.3118	0.018506	13.038
Exponential	0.39187	1550	1.0233	0.0062741	17.956

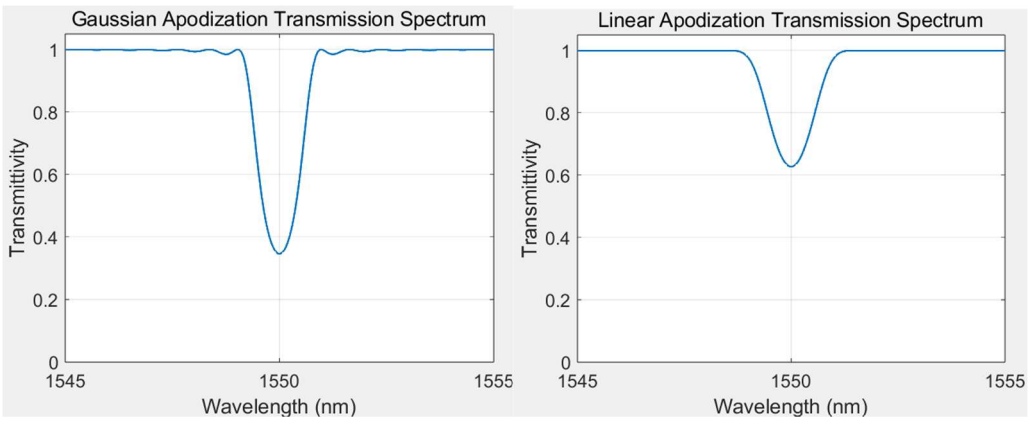
As listed in Table 1, the peak wavelengths of the four apodized gratings are all located at 1550 nm. This result confirms that the apodization profile mainly affects the spectral shape, while the central operating wavelength is still determined by the Bragg condition. Among the four cases, Gaussian apodization gives the highest peak reflectivity, with a value of 0.65327. The higher reflectivity suggests that the Gaussian profile retains a relatively strong coupling strength in the central part of the grating, where the main contribution to Bragg reflection is generated.

For the linear and cosine apodization functions, the peak reflectivity is approximately 0.37246. This value is much lower than that of the Gaussian case, showing that these two profiles reduce not only the coupling strength near the grating ends, but also the effective coupling strength over the whole grating region. As a result, the main reflection peak becomes weaker. The cosine apodization produces the largest 3-dB bandwidth, reaching 1.3118 nm. However, its sidelobe suppression ratio is 13.038 dB, which is the lowest among the four cases. Under the parameter settings used in this work, the cosine profile therefore tends to broaden the reflection band at the cost of weaker sidelobe suppression.

The exponential apodization shows a different tendency. Its peak reflectivity is 0.39187, lower than that of the Gaussian case, whereas its maximum sidelobe is reduced to 0.0062741. The corresponding sidelobe suppression ratio reaches 17.956 dB, which is the highest value in Table 1. This means that the exponential profile is effective in suppressing sidelobes, but part of the main-peak reflection efficiency is lost at the same time.

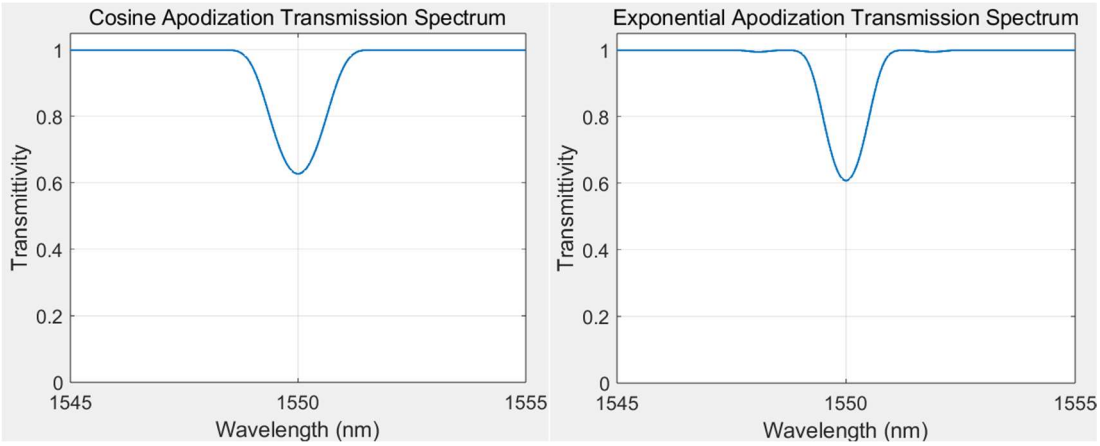
Based on these comparisons, Gaussian apodization provides a more balanced performance among peak reflectivity, bandwidth, and sidelobe suppression. Exponential apodization is more suitable when low sidelobe level is the primary design target and a moderate reduction in peak reflectivity is acceptable. Linear and cosine apodization functions show more evident trade-offs between reflection strength and spectral bandwidth. Therefore, for the grating length, refractive-index modulation depth, and apodization parameters used in this work, Gaussian apodization can be selected as the preferred scheme in terms of overall spectral performance.

5.4. Transmission Spectrum Analysis



(a) (b)

ISSN: 2664-9640



(c) (d)

Figure 6. Comparison of transmission spectra for different apodization functions

Table 2. Comparison of transmission spectrum performance parameters for different apodization functions

Apodization	Tmin	λ_B /nm	NotchWidth/nm	Extinction/dB
Gaussian	0.34673	1550	1.0819	4.6001
Linear	0.62754	1550	1.1613	2.0236
Cosine	0.62754	1550	1.3118	2.0236
Exponential	0.60813	1550	1.0233	2.1600

Following the reflection-spectrum results, the transmission response of the four apodized gratings is examined next. For a low-loss Bragg grating, reflection and transmission are closely related. As the incident wavelength approaches the Bragg wavelength, the forward mode is increasingly coupled to the backward mode, which produces a reduction in transmitted power and forms a stopband around the design wavelength.

The calculated transmission spectra are presented in Fig. 6. The Gaussian-apodized result is shown in Fig. 6(a). A clear transmission dip is observed around 1550 nm, in agreement with the location of the main reflection peak. Among the four profiles, the Gaussian case gives the lowest transmission level in the stopband, indicating that a larger fraction of the incident power is suppressed around the Bragg wavelength.

The transmission response obtained with linear apodization is given in Fig. 6(b). Its minimum transmission is higher than that of the Gaussian case, corresponding to a weaker reflection effect within the stopband. The transition around the central wavelength remains relatively smooth, although the lower effective coupling strength results in a less pronounced transmission notch.

Figure 6(c) shows the result for cosine apodization. The gradual change in coupling coefficient produces a relatively broad transition region in the transmission spectrum. At the same time, the depth of the transmission notch is smaller than that obtained with Gaussian apodization. This behavior is consistent with the lower reflection peak observed for the same apodization profile.

The exponential-apodized spectrum is plotted in Fig. 6(d). Its rapid reduction in coupling strength near the grating boundaries helps suppress spectral oscillations, but also limits the effective interaction region. As a result, the transmission notch is not as deep as that of the Gaussian case, which is consistent with the lower peak reflectivity obtained from the reflection-spectrum analysis.

ISSN: 2664-9640

The corresponding numerical results are summarized in Table 2. For all four apodization profiles, the minimum transmission remains centered at approximately 1550 nm. This further indicates that the apodization mainly changes the spectral shape and stopband response, while the central Bragg wavelength is largely preserved. The Gaussian-apodized grating has the lowest minimum transmission, with a value of 0.34673, and gives an extinction ratio of 4.6001 dB. These values indicate comparatively strong suppression of transmitted power around the Bragg wavelength.

The linear and cosine profiles have higher minimum-transmission values and therefore produce shallower transmission notches. The exponential case falls between these profiles in terms of extinction performance. Its stronger suppression of spectral oscillations is accompanied by a reduction in effective coupling near the grating boundaries, which limits the depth of the transmission stopband.

The transmission results are consistent with the trends observed in the reflection spectra. In particular, changes in the apodization profile affect the coupling strength distribution and consequently alter the reflection peak, transmission notch, bandwidth, and sidelobe characteristics. These parameters therefore need to be considered together when evaluating the spectral performance of the different apodization schemes.

5.5. Discussion

The role of apodization can be understood in terms of the spatial distribution of the grating coupling coefficient. In a uniform grating, the coupling coefficient is approximately constant over the grating region and drops sharply at the two ends, giving a profile similar to a rectangular window. The discontinuities at these boundaries introduce additional spectral components and are associated with the sidelobes observed in the reflection spectrum. Apodization changes this spatial profile by allowing the coupling strength to decrease gradually toward the grating ends. In this sense, the apodization function acts as a weighting function on the coupling coefficient, reducing the abrupt spatial transitions and thereby lowering the sidelobe components in the spectrum.

The refractive-index modulation in a point-loaded Bragg grating is produced by a sequence of discrete loading elements. In the present work, these individual structures are not modeled using a three-dimensional full-wave simulation. Instead, the effect of the discrete loading is incorporated into an equivalent coupling coefficient within the coupled-mode-theory and transfer-matrix framework. The resulting spatial variation is described by a continuous function, which makes it possible to examine different apodization profiles without explicitly calculating the electromagnetic response of every loading element. This approximation reduces the computational burden while retaining the main spectral effects associated with changes in the spatial coupling distribution.

The simulated spectra show that the choice of apodization profile has a noticeable influence on peak reflectivity, bandwidth, and sidelobe suppression. The Gaussian profile produces the highest peak reflectivity among the four cases while still providing appreciable sidelobe reduction. The exponential profile, in comparison, gives a lower main reflection peak but achieves the largest sidelobe suppression ratio. This difference reflects the trade-off between preserving strong coupling in the central part of the grating and reducing the coupling more strongly near its boundaries. The linear and cosine profiles produce lower reflection peaks under the present parameter conditions.

For the parameters considered in this study, the Gaussian profile provides a relatively balanced combination of reflection strength and sidelobe suppression. The exponential profile becomes more suitable when sidelobe reduction is given greater weight, even though this is accompanied by a reduction in peak reflectivity. These observations can be used as a reference

ISSN: 2664-9640

when selecting the apodization profile and further adjusting the structural parameters of point-loaded Bragg gratings.

6. Conclusion

In this work, an equivalent apodization analysis model suitable for point-loaded Bragg gratings is established based on coupled-mode theory and the transfer matrix method. The reflection and transmission spectral characteristics under four apodization functions, namely Gaussian, linear, cosine, and exponential apodization, are numerically simulated and comparatively analyzed. The results show that different apodization functions have significant effects on the peak reflectivity, 3-dB bandwidth, sidelobe suppression ratio, and transmission stopband depth of the grating.

First, compared with the uniform grating, apodization can effectively improve the spectral shape of the grating. By gradually reducing the coupling coefficient at both ends of the grating, the apodization function decreases the abruptness of the refractive-index modulation at the grating boundaries, thereby weakening the sidelobe oscillations on both sides of the main peak and improving the smoothness and spectral selectivity of the reflection spectrum.

Second, among the four apodization functions, Gaussian apodization exhibits better overall performance. The simulation results show that the Gaussian apodization has the highest peak reflectivity, reaching 0.65327, while its sidelobe suppression ratio is 16.334 dB. This indicates that Gaussian apodization can maintain a relatively high main-peak reflection strength while achieving effective sidelobe suppression. Although exponential apodization has a higher sidelobe suppression ratio, its peak reflectivity is lower than that of Gaussian apodization, indicating that it suppresses sidelobes at the expense of part of the main-peak reflection efficiency. Therefore, considering peak reflectivity, bandwidth, and sidelobe suppression performance, Gaussian apodization is more suitable as the preferred apodization function for point-loaded Bragg gratings under the parameter conditions used in this work.

Third, from the transmission spectrum results, the transmission dips corresponding to the four apodization functions are all located near 1550 nm, which is consistent with the peak wavelengths in the reflection spectra. This indicates that the apodization functions mainly change the spectral line shape and stopband characteristics of the grating, while they do not significantly alter the central Bragg wavelength. Among them, Gaussian apodization exhibits the lowest minimum transmittance and the highest extinction ratio, indicating that it also has strong stopband suppression capability in the transmission spectrum, which is consistent with the reflection spectrum analysis.

Finally, the equivalent modeling method based on $\kappa(z)$ adopted in this work can transform the discrete structural modulation in point-loaded gratings into a continuous coupling coefficient distribution. This enables unified analysis of different apodization functions within the transfer matrix framework. The proposed method has a clear calculation process and explicit physical meaning, and can provide a theoretical reference for reflection spectrum optimization, sidelobe suppression, and on-chip filter design of integrated optical waveguide gratings. Future work may further combine practical layout structures and full-wave simulation methods to investigate the geometric parameters, fabrication tolerances, and actual loss factors of point-loaded gratings in greater depth.

References

[1] Blumenthal, D. J., Heideman, R., Geuzebroek, D., Leinse, A., & Roeloffzen, C. (2018). Silicon nitride in silicon photonics. Proceedings of the IEEE, 106, 2209–2231.

ISSN: 2664-9640

[2] Hill, K. O., Fujii, Y., Johnson, D. C., & Kawasaki, B. S. (1978). Photosensitivity in optical fiber waveguides: Application to reflection filter fabrication. Applied Physics Letters, 32, 647–649.

[3] Erdogan, T. (1997). Fiber grating spectra. Journal of Lightwave Technology, 15, 1277–1294.

[4] Kashyap, R. (2009). Fiber Bragg gratings (2nd ed.). Academic Press.

[5] Lihachev, G., Riemensberger, J., Weng, W., et al. (2022). Low-noise frequency-agile photonic integrated lasers for coherent ranging. Nature Communications, 13, 3522.

[6] Liu, Y., Qiu, Z., Ji, X., et al. (2022). A photonic integrated circuit-based erbium-doped amplifier. Science, 376, 1309–1313.

[7] Halir, R., Cheben, P., Schmid, J. H., Bock, P. J., Wangüemert-Pérez, J. G., Ortega-Moñux, A., Alonso-Ramos, C., Molina-Fernández, Í., & Xu, D. X. (2015). Waveguide sub-wavelength structures: A review of principles and applications. Laser & Photonics Reviews, 9, 25–49.

[8] Kogelnik, H. (1969). Coupled wave theory for thick hologram gratings. The Bell System Technical Journal, 48, 2909–2947.

[9] Cheng, R., Jaeger, N. A. F., & Chrostowski, L. (2020). Fully tailorable integrated-optic resonators based on chirped waveguide Moiré gratings. Optica, 7, 647–657.

[10] Ji, X., Roberts, S., Corato-Zanarella, M., et al. (2021). Methods to achieve ultra-high quality factor silicon nitride resonators. APL Photonics, 6, 071101.